Proceedings of the Canadian Society for Mechanical Engineering International Congress 2021
CSME Congress 2021
June 27-30, 2021, Charlottetown, PE, Canada

Injecting a Viscoplastic Fluid in a Channel Filled with a Lower Density Newtonian Fluid: Effects of Premixing

Abdallah Ghazal
Department of Mechanical, Industrial and Aerospace Engineering
Concordia University
Montreal, Canada
ab_ghaza@encs.concordia.ca

Ida Karimfazli
Department of Mechanical, Industrial and Aerospace Engineering
Concordia University
Montreal, Canada
ida.karimfazli@concordia.ca

***Abstract*—Oil wells are normally abandoned using several cement plugs. Plugs above the deepest one are called off-bottom. The balanced plug method is the most used technique to place off-bottom plugs. In most cases, the initial stage of the balanced plug method includes injection of the cement slurry in cased wells. A tube smaller than the casing is inserted to the depth where the plug should be placed. Cement slurry is then injected through the tube into the cased wellbore, that is initially filled with wellbore liquids. Under field conditions, mixing of the fluids inside the injector is inevitable.**

In this study, we model the above cement injection process in a representative two-dimensional domain. We explore the effect of fluids premixing inside the injector on the dynamics below it. We first consider an idealized case where the displacing fluid fills the injector initially. To model the fluids premixing, we consider three other cases where the injector is initially filled with the displaced fluid, a buffer layer of both fluids and a combination of both.

Our preliminary results show that the injection in the idealistic case results in a cement finger developing below the injector. The finger then breaks due to an interfacial instability. As a result, a mixed layer forms below the injector. The premixing of fluids in the injector result in qualitatively similar dynamics as above. Mixed fluids advect below the injector. Shortly after, unsteady dynamics, within the injector or below it, facilitate the formation of a mixed layer below the injector.

***Index Terms*—Plug and Abandonment, Displacement flow, Viscoplastic fluid, Premixing**

I. Introduction

Oil and gas wells are classified based on their production status to *active* and *inactive* [1]. Active wells are the ones producing oil and gas economically. Wells that do not produce oil and gas in 12 months, however, are considered inactive [1]. Companies can either close inactive wells temporarily (i.e. *suspend*) or permanently (i.e. *abandon*) [2]. As of July 2019, the province of Alberta in Canada had $\sim 75,000$ suspended wells and $\sim 42,000$ abandoned [3]. The numbers then represented $\sim 25\%$ and $\sim 14\%$ of the registered wells in the province, respectively [3]. The cost of abandoning an oil well can be anywhere from $\sim 10,000\$$ to $\sim 1,000,000\$$, depending on the geographic location, depth and site conditions [4]. In 2019, the average cost of plugging a well in Alberta was $\sim 29,000\$$ [5]. Abandonment jobs that are not done properly incur significant additional costs [6].

This research is funded by NSERC and PETAC

Although there is much diversity in the abandonment protocols of the regulatory body across the globe, the goal of the process is to eliminate the potential risks to the environment [2], [6]. Recent studies, however, showed that abandoned wells are leaking Methane [7]–[9]. Improper placement of plugs may be considered as one of the possible reasons for such leaks. This study in motivated by common abandonment practices in Canada. In most cases, several plugs are placed along the well to ensure proper isolation to the perforated formations so that the well integrity is maintained. Plugs above the bottom one are often called *off-bottom*. The balanced plug method is the most used technique to place such plugs. A tube of smaller size compared the cased wellbore is positioned at the target location, where the off-bottom plug should be placed. Cement slurry is then injected into the well (see Fig.1). The aim here is for the heavy cement slurry to accumulate on a layer of a lower density wellbore fluids. While it may seem hydrodynamically infeasible, there is an anecdotal evidence of successful placement following this procedure [10].

Displacement flows in confined geometries are well studied for Newtonian fluids [11]–[14]. Problems involving non-Newtonian fluids, however, are less systematically explored. Taghavi et. al [15] and Alba et. al [16] conducted experimental studies of the displacement of a viscoplastic fluid by a higher density Newtonian fluid in a pipe for a wide range of inclination angles. Two primary flow regimes, *central* and *slump* flows, were observed. The authors also revealed different unsteady flows for high inclinations from horizontal. Zare et. al [17], [18] examined both density stable and unstable displacement flows numerically. The authors considered an upwards injection of a Newtonian fluid in a channel filled with a viscoplastic fluid. Amiri et. al [19], conducted both experimental and theoretical studies on the downward displacement flows in a vertical geometry. The authors used a Newtonian

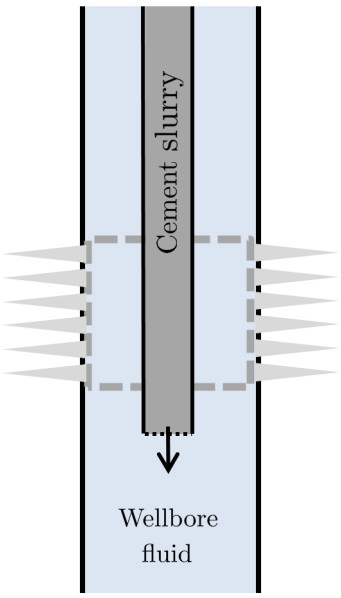

Fig. 1: An illustrative schematic of an idealistic injection stage of the balanced plug method. The dashed rectangle refers to the target location of the off-bottom plug. Note: the schematic is not to scale.

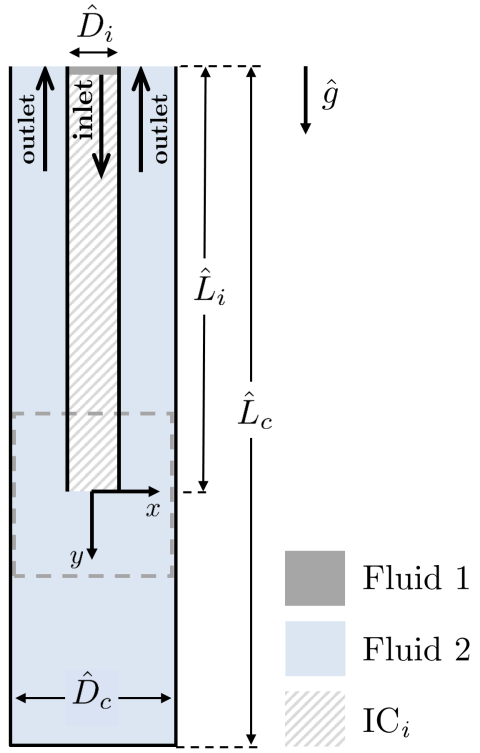

Fig. 2: Simplified illustrative schematic for the computational domain. The dashed rectangle represents the target plug position. The slanted lines for IC$_i$ represent a generalized initial condition for the fluids in the injector, see Fig.3 for the cases considered. Note: the schematic is not to scale.

fluid to displace a slightly lower density viscoplastic fluid. The results showed both static and moving residual layers. Both stable and unstable flows were reported for the latter cases.

Evidently, the studies on displacement flows are not representatives of neither the geometry nor the conditions of the cement injection stage in the balanced plug method (see Fig.1). In this study, therefore, we model the injection of a viscoplastic fluid into a channel initially filled with a lighter Newtonian fluid. We focus on the effects of the fluids premixing inside the injector on the dynamics below it.

II. Problem Setup

We model the injection process in a representative two-dimensional channel as illustrated in Fig. 2. The aspect ratio of the computational domain ($\hat{L}_c/\hat{D}_c$) is 90, where $\hat{L}_c$ and $\hat{D}_c$ are the casing length and width, respectively. We consider a fixed width ratio between the injector and the casing ($\hat{D}_i/\hat{D}_c = 0.5$). Also, the ratio between the injector and casing lengths ($\hat{L}_i/\hat{L}_c$) is 0.5. Fluid 1 is viscoplastic fluid and fluid 2 is Newtonian. Initially, the casing is filled with fluid 2. The slanted area in Fig. 2 indicates the region where different initial conditions are considered to explore the effect of premixing in the injector.

To facilitate the introduction of the initial conditions, we define the phase fraction field based on the mixture density, $\hat{\rho}$,

$$\phi = \frac{\hat{\rho} - \hat{\rho}_o}{\Delta\hat{\rho}}$$

where $\hat{\rho}_0 = (\hat{\rho}_1 + \hat{\rho}_2)/2$ is the reference density and $\Delta\hat{\rho} = \hat{\rho}_1 - \hat{\rho}_2$ is the density difference, $\hat{\rho}_1$ is the density of the displacing fluid (fluid 1) and $\hat{\rho}_2$ is the density of the displaced fluid (fluid 2). We use $\hat{\cdot}$ to denote a dimensional quantity. The phase fraction value for pure fluid 1 is thus 0.5, and the phase fraction value for fluid 2 is -0.5. We consider four different initial conditions for the phase fraction inside the injector (see Fig.3):

(I) constant at $\phi = 0.5$ (fluid 1),
(II) linear decrease between the injector inlet ($\phi = 0.5, y = -45$) and outlet ($\phi = -0.5, y = 0$),
(III) linear decrease between the injector inlet ($\phi = 0.5, y = -45$) and its half length ($\phi = -0.5, y = -22.5$), followed by a constant value ($\phi = -0.5$) till the injector outlet ($y = 0$),
(IV) constant at $\phi = -0.5$ (fluid 2).

The mathematical representations of the initial phase fraction fields in the injector are illustrated in Table I.

No-slip and no-penetration are applied on the walls. Fluid 1 is injected at the inlet with a uniform velocity. We assume the flow to be fully developed at the outlets.

A. Governing Equations

For the length and velocity scales we use the casing width ($\hat{D}_c$) and average inlet velocity ($\hat{V}_o$), receptively. The dimensionless variables become:

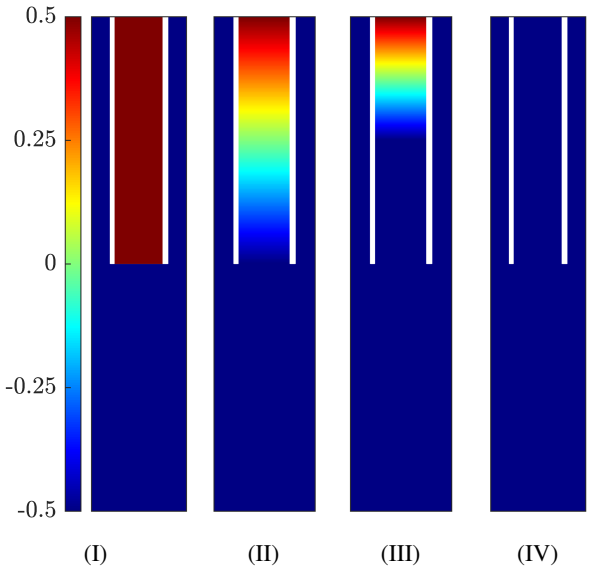

Fig. 3: Illustration of the presented fluids in the injector initially (IC_i). The colors refer to the phase fraction (ϕ). The displayed colormaps show the full length of the computational domain, $-45 \leq y \leq 45$. The white color represents the injector walls. (a) injector filled with fluid 1, (b) injector filled with a linear gradient between fluids 1 and 2, (c) the top half of the injector is similar to (b) and the other half is filled with fluid 2, (d) injector filled with fluid 2.

TABLE I: Mathematical Representations of the Initial Phase Fraction Fields in the Injector

IC_i Case[a]	***Injector Initial Phase Fraction Fields***
(I)	0.5 for $-L_i \leq y \leq 0$
(II)	$\frac{-1}{L_i}y - 0.5$ for $-L_i \leq y \leq 0$
(III)	$\begin{cases} \frac{-2}{L_i}\left(y + \frac{L_i}{2}\right) - 0.5 & \text{if } -L_i \leq y \leq \frac{-L_i}{2} \\ -0.5 & \text{if } \frac{-L_i}{2} < y \leq 0 \end{cases}$
(IV)	-0.5 for $-L_i \leq y \leq 0$

[a]See Fig.3 for visual representations. The injector width is $|x| \leq D_i/2$

$$x_i = \frac{\hat{x}_i}{\hat{D}_c}, \quad t = \frac{\hat{V}_o \hat{t}}{\hat{D}_c}, \quad u_i = \frac{\hat{u}_i}{\hat{V}_o}, \quad P = \frac{\hat{P}}{\hat{\rho}_o \hat{V}_o^2},$$
$$\tau_{ij} = \frac{\hat{\tau}_{ij}}{\hat{\rho}_o \hat{V}_o^2}, \quad \dot{\gamma}_{ij} = \frac{\hat{\dot{\gamma}}_{ij} \hat{D}_c}{\hat{V}_o}, \quad \mu = \frac{\hat{\mu}}{\hat{\rho}_o \hat{V}_o \hat{D}_c}.$$

where $(x_1, x_2) = (x, y)$, P is pressure, t is time, u_i is the fluid velocity in the x_i direction, τ_{ij} represents the deviatoric stress tensor, $\dot{\gamma}_{ij}$ represents the strain rate tensor and μ is the dynamic viscosity of the mixture.

The governing equations become:

$$(2At\phi + 1)\left[\frac{\partial u_i}{\partial t} + u_j \frac{\partial u_i}{\partial x_j}\right] = -\frac{\partial P}{\partial x_i} + \frac{\partial \tau_{ij}}{\partial x_j} - \frac{2At}{Fr^2}\phi\delta_{i2} \tag{1}$$

$$2At\left[\frac{\partial \phi}{\partial t} + u_i \frac{\partial \phi}{\partial x_i}\right] + (2At\phi + 1)\frac{\partial u_i}{\partial x_i} = \frac{2At}{Pe}\frac{\partial^2 \phi}{\partial x_i \partial x_i} \tag{2}$$

where At is the Atwood number, Fr is the Froude number, Pe is the Peclet number, and δ_{i2} is the kronecher delta.

We model the viscoplastic fluid using the Bingham constitutive law:

$$\begin{cases} \tau_{ij} = 2\left[\frac{1}{Re} + \frac{Bn}{2\dot{\gamma}}\right]\dot{\gamma}_{ij} & \text{if } \tau > Bn \\ \dot{\gamma}_{ij} = 0 & \text{if } \tau \leq Bn \end{cases} \tag{3}$$

where Bn is the Bingham number, Re is the Reynolds number, τ and $\dot{\gamma}$ are the second invariants of strain rate and shear stress tensors,

$$\dot{\gamma} = \sqrt{\frac{1}{2}\dot{\gamma}_{ij}\dot{\gamma}_{ij}}, \quad \tau = \sqrt{\frac{1}{2}\tau_{ij}\tau_{ij}}$$

We define the strain rate as: $\dot{\gamma}_{ij} = \frac{1}{2}\left[\frac{\partial u_i}{\partial x_j} + \frac{\partial u_j}{\partial x_i}\right]$.

When $\tau = Bn$, the Bingham model is non-differentiable. We therefore regularise the Bingham model following Bercovier-Engelman [20].

$$\begin{aligned} \tau_{ij} &= 2\mu_{1,e}\dot{\gamma}_{ij} \\ \mu_{1,e} &= \left[\frac{1}{Re} + \frac{Bn}{\sqrt{\epsilon^2 + (2\dot{\gamma})^2}}\right] \end{aligned} \tag{4}$$

Here $\mu_{1,e}$ is the effective viscosity of the viscoplastic fluid and ϵ is the regularization parameter.

The mixture viscosity is approximated by a linear function of the phase fraction,

$$\mu = (0.5 + \phi)\mu_{1,e} + (0.5 - \phi)\frac{m}{Re} \tag{5}$$

where m is the viscosity ratio.

We show the definitions and values of the above dimensionless numbers in Table II. The Reynold number (Re) and viscosity ratio (m) are chosen such that case I (i.e. idealistic case) is representative of a laminar flow below the injector in off-bottom plug placement. The values of the remaining dimensionless groups are chosen consistent with the practical ranges. We note here that the effective Peclet number (Pe) is typically orders of magnitude higher than the values associated with the molecular diffusion.

TABLE II: Definitions and Values of the Dimensionless Groups from the Governing Equations. $\hat{D}$ is the diffusion coefficient, $\hat{g}$ is the gravitational acceleration, $\hat{\tau}_y$ is the yield stress, $\hat{\mu}_1$ is the plastic viscosity of the displacing fluid (fluid 1) and $\hat{\mu}_2$ is the dynamic viscosity of the displaced fluid (fluid 2).

Dimensionless Group	***Value***
$At = \dfrac{\Delta\hat{\rho}}{2\hat{\rho}_o}$	0.130
$Fr = \dfrac{\hat{V}_o}{\sqrt{\hat{g}\hat{D}_c}}$	0.395
$Pe = \dfrac{\hat{V}_o\hat{D}_c}{\hat{D}}$	2.8×10^3
$Bn = \dfrac{\hat{\tau}_y}{\hat{\rho}_o\hat{V}_o^2}$	0.0027
$Re = \dfrac{\hat{\rho}_o\hat{V}_o\hat{D}_c}{\hat{\mu}_1}$	527
$m = \dfrac{\hat{\mu}_2}{\hat{\mu}_1}$	1.3

B. Numerical Method and Validation

The simulations are carried out using OpenFOAM v6 from the OpenFOAM Foundation. The software is based on the finite volume method. Since our problem involves two miscible incompressible fluids, we use the multiphase solver, *twoLiquidMixingFoam*. The solver algorithm is a combination of PISO (Pressure Implicit with Splitting of Operator) and SIMPLE (Semi-Implicit Method for Pressure-Linked Equations). The Bercovier-Engelman viscosity model is added in a user-defined script. Our space discretization is second order accurate, and our time discretization is first order implicit. We validated our simulations of unsteady flows in [21].

III. Results and Discussions

We show the dynamics following the injection of a heavy viscoplastic fluid in a lower density Newtonian fluid. We consider four different scenarios for the fluids that initially fill the injector. We focus our discussion on the dynamics below the injector and explore if they may differ as a result of the premixing inside the injector.

In Fig.4, we show snapshots of the phase fraction colormaps for case I, where fluid 1 initially fills the entire injector. Following the onset of injection, a viscoplastic finger develops below the injector and advects downstream (see Fig.4, $t = 15, 20$). Waves then appear at the interface between the two fluids (see Fig.4, $t = 25$). The waves evolve over time and break the viscoplastic finger. Vortices develop behind the broken finger as it travels downstream (see e.g. Fig.4, $t = 30$). A mixing layer thus forms below the injector (see Fig.4, $t = 50$). After the broken finger is diffused, the mixing layer reaches a qualitatively quasi-steady length (see Fig.4, $t = 70, 90, 100$). The mixed layer reduces the local buoyant forces such that the injected fluid diverts into the gap between the injector and channel walls.

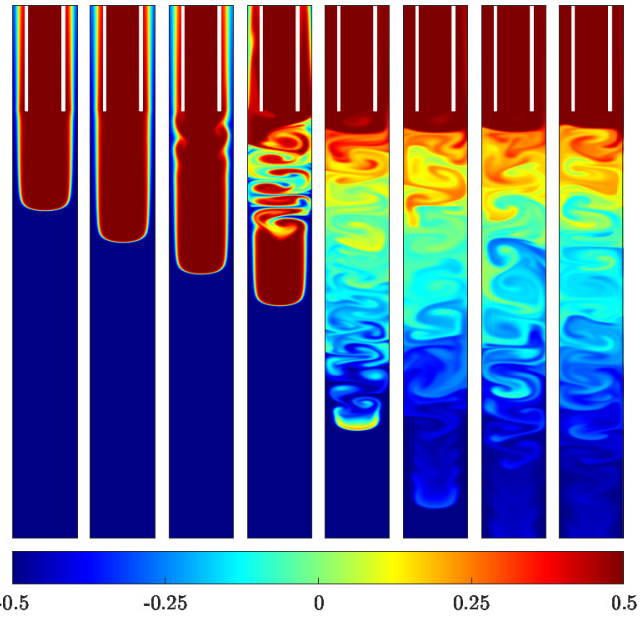

Fig. 4: Phase fraction color maps for case I, where the injector is initially filled with fluid 1 (see Fig. 3I for the initial condition). For the values of the dimensionless groups, see table II. The successive non-dimensional snapshot times from left to right are $t = 15, 20, 25, 30, 50, 70, 90, 100$. Blue color refers to the Newtonian fluid ($\phi = -0.5$), while the red color refers to the viscoplastic ($\phi = 0.5$). The white color represents the injector walls. The displayed colormaps show a fraction of the computational domain, $-5 \leq y \leq 20$.

Fig.5 shows snapshots of the phase fraction field for case II (the initial condition is illustrated in Fig.3II). A finger of mixed fluids, with a relatively low phase fraction of the viscoplastic fluid, appears below the injector shortly after the injection onset (see Fig.5, $t = 3$). The phase fraction of the fluids within the finger increases as it advects downstream (see Fig.5, $t = 10, 15$). The downstream advection of the finger is destabilized shortly after, leading to the finger breakup and enhancing the mixing below the injector (see Fig.5, $t = 20, 25, 30$). At later times, the viscoplastic fluid wipes out all the mixed fluids in the injector.

A qualitative comparison between cases I and II for the front travelled distance over the same time interval suggests that the advective front velocity is higher in case I. This is not surprising as buoyancy effects are stronger in case I. We also note that the quasi-steady mixing layer of case II has a high density gradient near the injector tip and a relatively short length compared to case I (see Fig.5, $t = 70, 100$).

Fig.6 shows snapshots of the phase fraction for case III (the initial condition is illustrated in Fig. 3III). Initially, a finger appears to start forming below the injector. Similar to

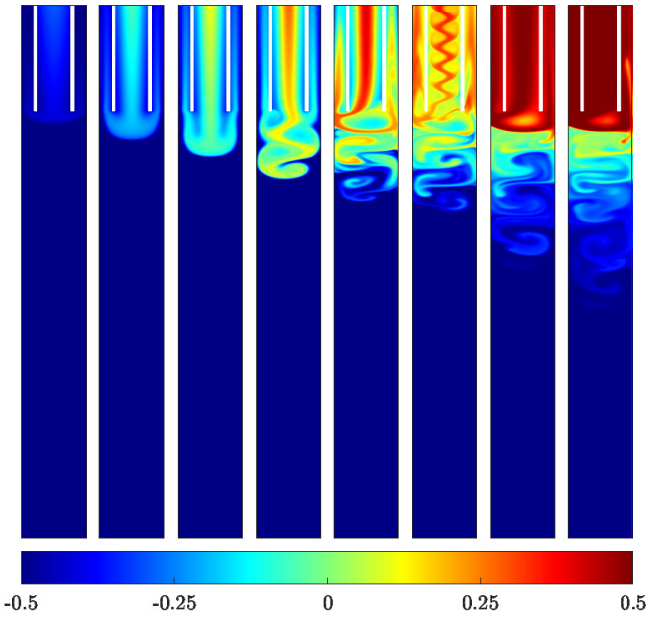

Fig. 5: Phase fraction color maps for case II (see Fig.3II for the initial condition). For the values of the dimensionless groups, see table II. The successive non-dimensional snapshot times from left to right are $t = 3, 10, 15, 20, 25, 30, 70, 100$. Blue color refers to the Newtonian fluid ($\phi = -0.5$), while the red color refers to the viscoplastic ($\phi = 0.5$). The white color represents the injector walls. The displayed colormaps show a fraction of the computational domain, $-5 \leq y \leq 20$.

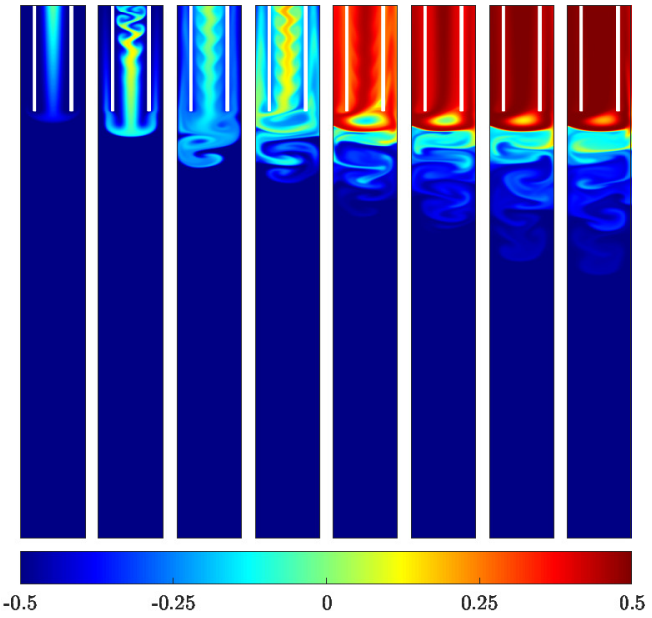

Fig. 6: Phase fraction color maps for case III (see Fig.3III for the initial condition). For the values of the dimensionless groups, see table II. The successive non-dimensional snapshot times from left to right are $t = 17, 20, 25, 30, 50, 70, 90, 100$. Blue color refers to the Newtonian fluid ($\phi = -0.5$), while the red color refers to the viscoplastic ($\phi = 0.5$). The white color represents the injector walls. The displayed colormaps show a fraction of the computational domain, $-5 \leq y \leq 20$.

case II, the phase fraction within the finger increases with time (see Fig.6, $t = 17, 20$). This flow regime is quickly destabilized, with apparent instabilities within and below the injector. Similar to the cases discussed before, the finger breakup leads to enhanced mixing below the injector and the formation of a quasi-steady mixing layer. The mixing continues as higher quality of mixed fluids emerge from the injector (see Fig.6, $t = 30$). The developed mixed layer in this case is similar to case II: it is short compared to case I and has a high density gradient close to the injection point. The mixing layer here also shows that it is reaching a quasi-steady state (see Fig.6, $t = 50, 70, 90, 100$).

In Fig.7, we show snapshots of the phase fraction colormaps for case IV, where fluid 2 initially fills the entire injector. Before $t = 30$, there is negligible mixing below the injector and the dynamics are unsteady in the injector. Shortly after, an unsteady stream of mixed fluids reaches the injector tip and advances downstream (see Fig.7, $t = 32, 35$). The dynamics below the injector then become unsteady, enhancing the mixing therein. A mixing layer forms as the phase fraction of the fluid streaming out of the injector increases (see Fig.7, $t = 38$). The mixing layer prevents the injected fluid from penetrating downstream (see Fig.7, $t = 50$). We also note that the mixed layer reaches a quasi-steady state. The length and phase fraction profile within the layer are similar to cases II and III (see Fig.7, $t = 70, 90, 100$).

The four illustrative cases investigated here reveal a few key similarities. Initially, fluids stream out of the injector and advect downstream. Unsteady dynamics then result in enhanced mixing below the injector, leading to the formation of a mixed layer therein. We note that the length and phase fraction profile of the mixing layer depend strongly on premixing of the fluids in the injector and the amount of advected fluids below it.

IV. Conclusions

In this study, we introduced a model problem to investigate the early stages of cement injection in off-bottom plugs. We modelled the cement slurry as a viscoplastic fluid and the wellbore liquid as Newtonian. We considered injecting a viscoplastic fluid into a channel filled with a Newtonian fluid, through an injector. We studied different initial phase fraction profiles within the injector, exploring four cases spanning a wide range of scenarios. For the idealistic case where the injector is initially filled with the viscoplastic fluid, a distinct finger develops below the injector and advances downstream. The finger then breaks due to interfacial instabilities. A mixing layer thus forms below the injector. We observed qualitatively similar dynamics for the other cases, where lower phase fraction fluids fill the injector initially. A low phase fraction

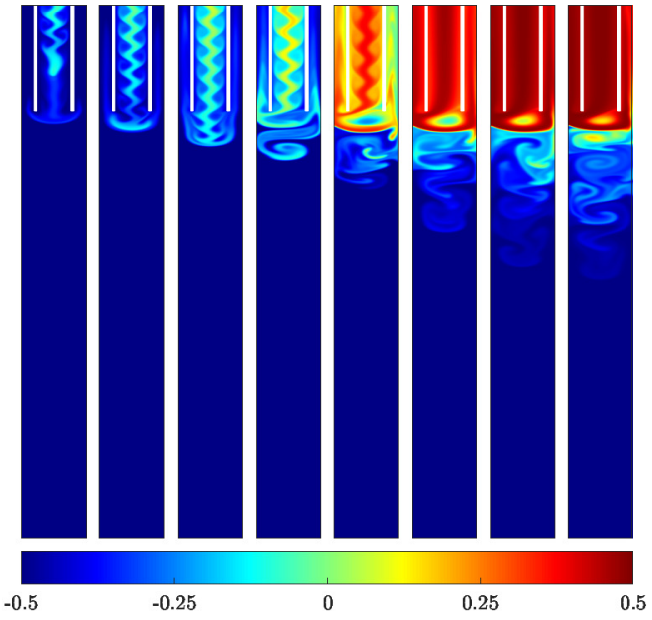

Fig. 7: Phase fraction color maps for case IV, where the injector is initially filled with fluid 2 (see Fig.3IV for the initial condition). For the values of the dimensionless groups, see table II. The successive non-dimensional snapshot times from left to right are $t = 30, 32, 35, 38, 50, 70, 90, 100$. Blue color refers to the Newtonian fluid ($\phi = -0.5$), while the red color refers to the viscoplastic ($\phi = 0.5$). The white color represents the injector walls. The displayed colormaps show a fraction of the computational domain, $-5 \leq y \leq 20$.

finger first emerge from the injector. Unsteady dynamics then facilitate the formation of the mixed layer below the injector. The mixed layer here has short length and high density gradient as compared to the idealistic case.

Future parametric studies will reveal the premixing effects on the contamination of the accumulated fluids above the injector.

ACKNOWLEDGMENT

This research has been carried out at Concordia University. The authors gratefully acknowledge the financial support provided by PTAC-AUPRF via grant PTAC-17-WARI-02 and from NSERC via grant CRDPJ 516022-17 ("Plug and Abandon Strategies for Canada's Oil & Gas Wells"). Abdallah Ghazal acknowledges the support of Le Fonds de recherche du Québec – Nature et technologies (FRQNT). This research was enabled in part by support provided by Calcul Québec (`http://www.calculquebec.ca`) and Compute Canada (`http://www.computecanada.ca`).

REFERENCES

[1] Life Cycle of a Well — Exploration — Well Abandonment — Reclamation.

[2] Suspension and Abandonment — Alberta Energy Regulator.

[3] Vanessa Alboiu and Tony R. Walker. Pollution, management, and mitigation of idle and orphaned oil and gas wells in Alberta, Canada. *Environmental Monitoring and Assessment*, 191(10):1–16, 2019.

[4] Mary Kang, Denise L. Mauzerall, Daniel Z. Ma, and Michael A. Celia. Reducing methane emissions from abandoned oil and gas wells: Strategies and costs. *Energy Policy*, 132:594–601, 2019.

[5] Orphan Well Association 2019 Report. Technical report, Orphan Well Association (OWA), Calgary, Alberta, 2019.

[6] Mari R. Tveit, Mahmoud Khalifeh, Tor Nordam, and Arild Saasen. The fate of hydrocarbon leaks from plugged and abandoned wells by means of natural seepages. *Journal of Petroleum Science and Engineering*, 196:108004, 2021.

[7] Stuart N. Riddick, Denise L. Mauzerall, Michael A. Celia, Mary Kang, and Karl Bandilla. Variability observed over time in methane emissions from abandoned oil and gas wells. *International Journal of Greenhouse Gas Control*, 100:103116, 2020.

[8] Eric D. Lebel, Harmony S. Lu, Lisa Vielstädte, Mary Kang, Peter Banner, Marc L. Fischer, and Robert B. Jackson. Methane Emissions from Abandoned Oil and Gas Wells in California. *Environmental Science and Technology*, 54(22):14617–14626, 2020.

[9] J. M. Abboud, T. L. Watson, and M. C. Ryan. Fugitive methane gas migration around Alberta's petroleum wells. *Greenhouse Gases: Science and Technology*, 2020.

[10] E. Trudel, M. Bizhani, M. Zare, and I. A. Frigaard. Plug and abandonment practices and trends: A British Columbia perspective. *Journal of Petroleum Science and Engineering*, 183(July):106417, 2019.

[11] S. M. Taghavi, T. Séon, K. Wielage-Burchard, D. M. Martinez, and I. A. Frigaard. Stationary residual layers in buoyant Newtonian displacement flows. *Physics of Fluids*, 23(4):044105, 2011.

[12] S. M. Taghavi, T. Séon, D. M. Martinez, and I. A. Frigaard. Influence of an imposed flow on the stability of a gravity current in a near horizontal duct. *Physics of Fluids*, 22(3):2–4, 2010.

[13] K. Alba, S. M. Taghavi, and I. A. Frigaard. Miscible density-stable displacement flows in inclined tube. *Physics of Fluids*, 24(12):123102, 2012.

[14] S. Akbari and S. M. Taghavi. Injection of a heavy fluid into a light fluid in a closed-end pipe. *Physics of Fluids*, 32(6):063302, 2020.

[15] S. M. Taghavi, K. Alba, M. Moyers-Gonzalez, and I. A. Frigaard. Incomplete fluid-fluid displacement of yield stress fluids in near-horizontal pipes: Experiments and theory. *Journal of Non-Newtonian Fluid Mechanics*, 167-168:59–74, 2012.

[16] K. Alba, S. M. Taghavi, John R. de Bruyn, and I. A. Frigaard. Incomplete fluid-fluid displacement of yield-stress fluids. Part 2: Highly inclined pipes. *Journal of Non-Newtonian Fluid Mechanics*, 201:80–93, 2013.

[17] M Zare, A Roustaei, and I A Frigaard. Buoyancy effects on micro-annulus formation: Density stable displacement of Newtonian–Bingham fluids. *Journal of Non-Newtonian Fluid Mechanics*, 247:22–40, 2017.

[18] M. Zare and I. A. Frigaard. Buoyancy effects on micro-annulus formation: Density unstable Newtonian–Bingham fluid displacements in vertical channels. *Journal of Non-Newtonian Fluid Mechanics*, 260:145–162, 2018.

[19] A. Amiri, A. Eslami, R. Mollaabbasi, F. Larachi, and S. M. Taghavi. Removal of a yield stress fluid by a heavier Newtonian fluid in a vertical pipe. *Journal of Non-Newtonian Fluid Mechanics*, 268:81–100, 2019.

[20] M. Bercovier and M. Engelman. A finite-element method for incompressible non-Newtonian flows. *Journal of Computational Physics*, 36(3):313–326, 1980.

[21] A. Ghazal and I. Karimfazli. Off-Bottom Plug Placement: How It Works? volume Volume 11: Petroleum Technology of *International Conference on Offshore Mechanics and Arctic Engineering*, 08 2020.